International Journal of Bioprinting

RESEARCH ARTICLE

Bacterial nanocellulose-reinforced gelatin methacryloyl hydrogel enhances biomechanical property and glycosaminoglycan content of 3D-bioprinted cartilage

Jinshi Zeng[1], Litao Jia[1], Di Wang[1], Zhuoqi Chen[1], Wenshuai Liu[1], Qinghua Yang[1]*, Xia Liu[1,2]*, Haiyue Jiang[1]*

[1]Research Center of Plastic Surgery Hospital, Chinese Academy of Medical Sciences and Peking Union Medical College, Beijing, 100144, PR China

[2]Key Laboratory of External Tissue and Organ Regeneration, Chinese Academy of Medical Sciences and Peking Union Medical College, Beijing, 100144, PR China

(This article belongs to the Special Issue: 3D Bioprinting with Photocurable Bioinks)

Abstract

Tissue-engineered ear cartilage scaffold based on three-dimensional (3D) bioprinting technology presents a new strategy for ear reconstruction in individuals with microtia. Natural hydrogel is a promising material due to its excellent biocompatibility and low immunogenicity. However, insufficient mechanical property required for cartilage is one of the major issues pending to be solved. In this study, the gelatin methacryloyl (GelMA) hydrogel reinforced with bacterial nanocellulose (BNC) was developed to enhance the biomechanical properties and printability of the hydrogel. The results revealed that the addition of 0.375% BNC significantly increased the mechanical properties of the hydrogel and promoted cell migration in the BNC-reinforced hydrogel. Constructs bioprinted with chondrocyte-laden BNC/GelMA hydrogel bio-ink formed mature cartilage in nude mice with higher Young's modulus and glycosaminoglycan content. Finally, an auricle equivalent with a precise shape, high mechanics, and abundant cartilage-specific matrix was developed *in vivo*. In this study, we developed a potentially useful hydrogel for the manufacture of auricular cartilage grafts for microtia patients.

Keywords: 3D bioprinting; Bacterial nanocellulose; Gelatin methacryloyl; Glycosaminoglycan content; Biomechanical property; Auricular cartilage

***Corresponding author:**
Haiyue Jiang
(jianghaiyue@psh.pumc.edu.cn)

Citation: Zeng J, Jia L, Wang D, *et al*., 2023, Bacterial nanocellulose-reinforced gelatin methacryloyl hydrogel enhances biomechanical property and glycosaminoglycan content of 3D-bioprinted cartilage. *Int J Bioprint*, 9(1): 631.
https://doi.org/10.18063/ijb.v9i1.631

Received: July 5, 2022

Accepted: July 22, 2022

Published Online: October 29, 2022

1. Introduction

In clinical practice, microtia is one of the most common congenital malformations. At present, autologous costal cartilage transplantation has become the most common treatment for microtia[1-5]. However, the complications caused by this operation, such as pneumothorax, post-operative pain, and chest wall deformity, are hardly inevitable. Moreover, the manually carved stent relies more on the technique of the surgeon, and there is no accurate shape for a stent[6,7].

Recent advances in regenerative medicine and tissue engineering have provided new hope for the treatment of microtia[8]. Professor Haiyue Jiang's team has successfully

applied tissue-engineered auricular cartilage based on polyglycolic acid/polylactic acid and chondrocytes to clinical practice[9]. However, it was found that the implants collapsed at varying degrees after some time. Polymer materials can easily cause aseptic inflammation[10], and it is challenging to achieve uniform distribution of chondrocytes in the scaffolds using the traditional seeding cell method[11]; these justify the unsatisfactory results. Due to their low aseptic inflammation, natural hydrogel materials such as alginate, gelatin, and hyaluronic acid have attracted attention recently[12-17]. The three-dimensional (3D) bioprinting technology has significant advantages in the construction of accurate anatomical contours because it can precisely define the spatial distribution of cells and materials[18,19]. Therefore, 3D bioprinting based on natural hydrogel materials is a promising approach to overcoming the bottleneck of cartilage tissue construction[15,20,21]. However, the insufficient mechanical stability of hydrogel materials makes it difficult to ensure the shape of the scaffold *in vivo*.

Gelatin methacryloyl (GelMA) is one of the commonly used hydrogels in 3D bioprinting, and it has been effectively applied to cartilage tissue engineering[22-24]. However, due to low mechanical properties, its printing fidelity is limited, and it is difficult to produce large-scale functional tissue constructs only using GelMA as the scaffold[25,26].

To improve the mechanical properties of the scaffold with natural materials, we propose adding bacterial nanocellulose (BNC) to GelMA to enhance the mechanical stability and printability of hydrogels for cartilage bioprinting. BNC is a type of naturally occurring high-molecular-weight polymer with good biocompatibility, high Young's modulus, excellent water retention, and good flexibility[27,28]. In addition, it has good printability and shear thinning characteristics, which make it suitable for 3D bioprinting[29]. In this study, we explored the appropriate proportion of BNC in the composite hydrogel and the feasibility of using this bio-ink to regenerate auricular cartilage with high mechanical performance *in vivo*.

2. Materials and Methods

2.1. Materials

Unless specified otherwise, all chemicals were obtained from Sigma-Aldrich (St. Louis, USA). GelMA lyophilized powder and lithium phenyl-2,4,6-trimethylbenzoylphosphinate solution (LAP; 2.5% w/v) were procured from SunP Biotech (Beijing, China). Bacterial cellulose (BC) was purchased from the Hainan Yide Food Co., Ltd. (Hainan, China), while Dulbecco's Modified Eagle Medium (DMEM), penicillin-streptomycin-neomycin antibiotic (PSN), and fetal bovine serum (FBS) were purchased from Gibco (Grand Island, NY, USA).

2.2. Animals

Japanese white rabbits (female, 2 months old) and nude mice (male and female, 6 weeks old) were bought from Beijing Vital River Laboratory Animal Technology Co., Ltd. (Beijing, China). All animal experiments were approved by the Institutional Animal Care and Use Committee of the Plastic Surgery Hospital (Approval ID: 2017 – 37).

2.3. Preparation of hydrogel materials

BNC was produced using BC as previously described[30]. In brief, BC was purified with 2% (w/v) NaOH at 80°C for 1 h and then washed repeatedly with distilled water until a neutral pH was obtained, was repeatedly hydrolyzed and centrifuged under acidic conditions to obtain BNC suspension, which was then dialyzed and freeze-dried to produce BNC powder. GelMA lyophilized powder and LAP were dissolved in Dulbecco phosphate-buffered saline (DPBS; Gibco, Grand Island, NY, USA) to form 10% w/v GelMA and 0.25% w/v LAP-based solutions, which were used in the control group. A certain proportion of irradiated BNC was added to the GelMA solution to form BNC/GelMA hydrogels with different concentrations (Table 1).

2.4. Compression test on hydrogels

Silicone elastomer bases (Slygard™ 184, Dowsil, USA) were heated at 70°C for 3 h to make a 10 × 4 mm disk mold. A 300 µl hydrogels were added into the mold and irradiated with 405 nm, 30 mW/cm^2 ultraviolet (UV) light for 10 s to make it completely cross-linked to form a cylindrical-shaped scaffold (10 × 4 mm) for compression test (n = 7). A biomechanical analyzer (Instron 5967, USA) with a 100 N pressure sensor was used for the compression tests. A constant compressive strain rate was maintained at 1 mm/min until 80% of maximal deformation had been reached. The hydrogels' Young's modulus was measured with the slope of the stress-strain curve set between 10% and 20% strain. A humidifier was used to maintain the surrounding air humid throughout the tests.

Table 1. Hydrogels content concentration

Groups	GelMA (% w/v)	BNC (% w/v)	LAP (% w/v)
10%GelMA	10	0	0.25
+0.075% BNC	10	0.075	0.25
+0.225% BNC	10	0.225	0.25
+0.375% BNC	10	0.375	0.25
+0.525% BNC	10	0.525	0.25

GelMA, Gelatin methacryloyl; BNC, Bacterial nanocellulose

2.5. Rheological analysis

The rheological tests were performed with an Anton-Paar MCR 302 rheometer (Anton-Paar GmbH, Austria) using a 25 mm diameter parallel plate (PP25, d = 1.0 mm). Temperature sweep test was conducted to evaluate the hydrogels' behavior at various temperatures by setting a temperature increase at a rate of 2°C/min in the range of 0 – 40°C, and the values of G' (storage modulus) and G" (loss modulus) were recorded for each temperature. Viscosity was measured as a function of shear rate (0.1 – 100 s^{-1}) at 21°C. All measurements were performed at 1 Hz and 1% strain[31].

2.6. Scanning electron microscopy (SEM) examination

Following lyophilization and gold sputter coating, samples were analyzed using a Quanta 2000 scanning electron microscope (FEI Co., The Netherlands) at 15 kV. ImageJ software (ImageJ Software Inc., USA) was used to analyze photomicrographs.

2.7. Printability test

3D printing was performed with the 3D-Bioplotter printer (EnvisionTec, Germany). The hydrogel was placed into the bioprinter barrel and incubated for 10 min at 37°C before extrusion. The extrusion test was carried out at 21°C using various nozzles with inner diameters ranging from 150 μm to 600 μm.

The nozzle with a 400 μm inner diameter was used to print various models to test the printing resolution and precision of the composite hydrogel. The stereolithography (STL) files of the cube and the acronym PSH characters for plastic surgery hospital were built by AutoCAD software (Autodesk, San Rafael, CA). The human nose construction of the STL file was downloaded from an open-source website at https://www.thingiverse.com/, and the mandibular model bracket was provided by Envision-Tec. Subsequently, the STL files were imported into the slicing software Perfactory RP (EnvisionTec, Germany). The layer height was set as 320 μm and sliced in the model. The sliced model was imported into the 3D bioprinting system visual machine (EnvisionTec, Germany). In the printing system, the internal structure of the scaffolds was set as a cross grid, and the line spacing was set as 800 μm. The applied extrusion pressure for the composite hydrogel was 0.4 – 0.8 bar, and the nozzle speed was 3.5 – 4.5 mm/s (Table 2). The composite hydrogel was placed in the barrel of the 3D bio-printer and incubated at 21°C for 15 min before printing. Each stack of two layers was completely cross-linked by a 405 nm, 30 mW/cm^2 UV source for 10 s. During printing, images of each layer were collected using the inbuilt camera.

Table 2. 3D bioprinting parameters

Materials	10% w/v GelMA	10% w/v GelMA+0.375% BNC
Platform temperature (°C)	25	25
Barrel temperature (°C)	21	21
Ambient temperature (°C)	20–22	20–22
Printing speed (mm/s)	5.0–8.0	3.5–4.5
Printing pressure (Bar)	0.2–0.5	0.4–0.8

GelMA: Gelatin methacryloyl, BNC: Bacterial nanocellulose

2.8. Isolation and cultivation of auricular chondrocytes

As previously described[32], the ear cartilage of Japanese white rabbits was extracted and minced into 1 mm^3 pieces under sterile conditions. The cartilage fragments were digested with 0.2% type II collagenase solution for 8 h at 37°C, then filtered through a 100 μm filter screen. The chondrocytes were collected, cultivated, and expanded in culture medium containing high-glucose DMEM, 10% FBS, and 1% PSN with 5% carbon dioxide (CO_2) and 95% humidity at 37°C. Cells at second passage were collected and used for the subsequent experiments.

2.9. 3D bioprinting of cell-laden constructs

For building cell-laden constructs, 0.375% BNC, 10% GelMA, and 0.25% LAP were dissolved in culture medium as described above. The chondrocytes were collected and mixed into the hydrogels to make bio-ink with a concentration of 1 × 10^7 cells/mL. During printing, the extrusion pressure and printing speed were adjusted according to the material drawing state. After printing, the scaffolds were immersed in the culture medium and placed in the CO_2 incubator for culture.

2.10. Cell viability and migration assays

After being cultured *in vitro* for 1, 4, and 7 days, the Calcein-AM/PI Double Staining Kit (DOJINDO, Japan) was used to evaluate the viability of cells in hydrogels. The results were examined using Leica TCS SP8 CARS confocal microscope. ImageJ software was used to measure the cell viability in three randomly chosen visual fields.

To evaluate cell migration, BNC/GelMA and GelMA hydrogels were cross-linked on one side of 15 mm confocal Petri dish loaded with chondrocytes (1 × 10^6 cells/mL). Cell-free hydrogels were used to cover the opposite side of the Petri dish[33]. Following *in vitro* culture for 7 days, the Calcein-AM was used to stain the living cells, and a confocal microscope was used to observe cell migration.

2.11. Cartilage regeneration *in vivo*

Cell-laden constructs were cultivated *in vitro* for 1 day and then implanted into nude mice subcutaneously to observe cartilage formation *in vivo*. The samples were taken out at 4, 8, 12, and 24 weeks after implantation for biomechanical test, glycosaminoglycan (GAG) content test, total collagen content test, and histological examination.

2.12. Biomechanical and biochemical analysis of the regenerated cartilage

The compression tests of regenerated cartilage ($n = 3$) were performed by Instron 5967 with a 100 N pressure sensor as described above, and Young's modulus of the samples was measured based on the slope of the stress-strain curve set between 10% and 20% strain.

The dimethylmethylene blue GAG test kit (GenMed Scientifics Inc., Shanghai, China) was used to detect the GAG content in the samples ($n = 3$). Being a unique amino acid in collagen, hydroxyproline accounts for about 13.4% of the total content of collagen. The hydroxyproline detection kit (Nanjing Jiancheng Bioengineering Institute, Nanjing, China) was used to quantify the content of hydroxyproline in samples ($n = 3$). All operations were carried out according to previously established protocols[34].

2.13. Histological examination

Regenerated cartilages were collected and subjected to histological examinations. The samples were fixed in 4% paraformaldehyde, dehydrated, and embedded in paraffin. Hematoxylin and eosin (H&E), Alcian blue (Solarbio, China), and Safranine-O (Solarbio, China) staining were performed, as previously described, to evaluate the cartilage extracellular matrix deposition and histological structure in the regenerated cartilage[32].

2.14. Statistical analyses

GraphPad Prism 8.0 software was utilized for statistical analyses. All experimental data were obtained from at least three repeated experiments, and data are reported as means ± standard deviation. Statistical significance was evaluated by Student's *t*-test or one-way analysis of variance. Values of $P < 0.05$ were considered statistically significant. Data distribution should meet the normal distribution requirements.

3. Results and discussion

3.1. Selection of BNC proportion in the composite hydrogels

This study showed that BNC existed in suspension in 10% GelMA solutions after heating and mixing in the water bath because BNC is insoluble in water, and it would form a colloid or suspension in hydrogel[35]. With the increase of BNC ratio, the composite hydrogel became more turbid (Figure 1A). The stress-strain curves of each composite hydrogel sample showed that with the increase of BNC content, the slope of the curve gradually increased (Figure 1B). By calculating the slope of 0.1 – 0.2 mm/mm strain, Young's moduli of 10% GelMA, 0.075% BNC, 0.225% BNC, 0.375% BNC, and 0.525% BNC were 28.19 ± 3.058 kpa, 28.72 ± 2.066 kpa, 35.34 ± 1.430 kpa, 49.94 ± 2.775 kpa, and 53.74 ± 3.844 kpa, respectively (Figure 1C). From the 0.225% BNC group, Young's modulus of the hydrogels was significantly higher than that of 10% GelMA ($P < 0.001$) and increased with the increment of BNC concentration. However, there was no significant difference in Young's modulus between 0.375% BNC and 0.525% BNC ($P > 0.05$). In our opinion, when the BNC content is too high, its distribution in the solution becomes uneven, which may affect the full crosslinking of GelMA. Fourati *et al*. found that when nanocellulose was used as the additive phase, the mechanical properties of the composites would initially increase, but decreased after exceeding a certain amount[36]. In another study, Fan *et al*. also found that when cellulose nanocrystals (CNCs) were added to 15%, there was no significant difference between 10% CNC and 15% CNC when CNCs were used to strengthen GelMA/HAMA hydrogels[37]. Moreover, we found that the hydrogel with 0.525% BNC was difficult to be extruded and the nozzle could be blocked easily. Therefore, in the subsequent experiment, 0.375% BNC was selected as the experimental group (BNC/GelMA group), and 10% GelMA without BNC was set as the control group (GelMA group).

3.2. Characterization of hydrogels

3.2.1. Rheological test

We detected the gelatinization with temperature change and shear thinning behavior of the BNC/GelMA hydrogel by rheological analysis. We observed that at 0 – 40°C, G' (storage modulus) and G" (loss modulus) of both hydrogels decreased with the increase in temperature. At 0 – 23.5°C, when the storage modulus (G') dominated (G' > G"), both materials had gel-like properties. Conversely, at 23.5 – 40°C, when the loss modulus (G") dominated (G' < G"), the materials had liquid-like properties. Thus, 23.5°C was the common gel-forming point of these two materials (Figure 2A and B). The gelling temperature of the hydrogel did not change after BNC was added. In addition, it could be seen that both the BNC/GelMA group and the GelMA group have obvious shear thinning behavior at 21°C (Figure 2C). These results suggested that the BNC/GelMA hydrogel was suitable for 3D printing.

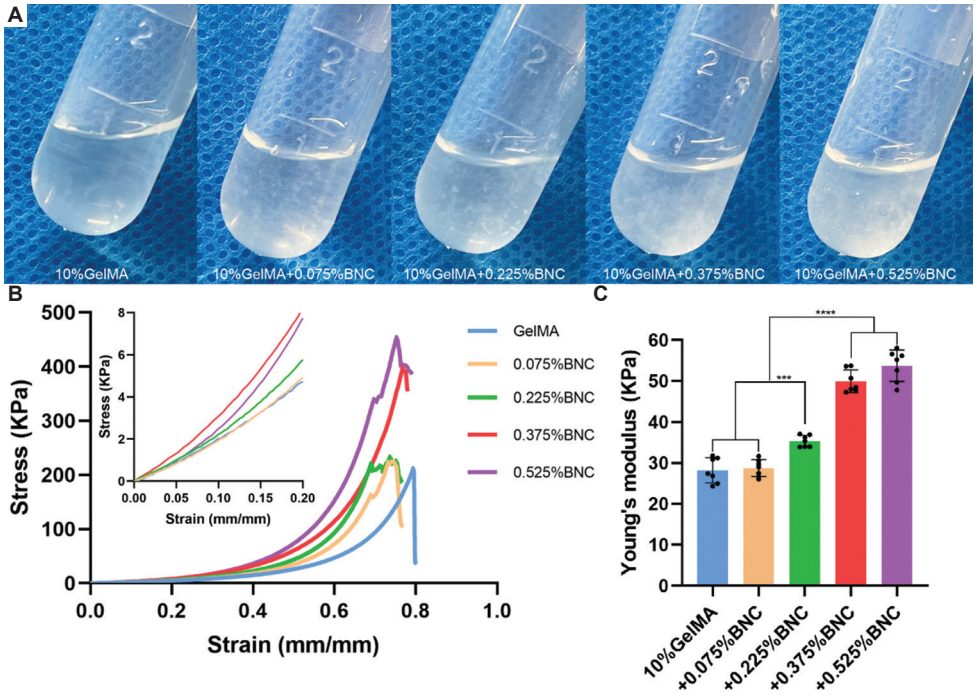

Figure 1. Preparation of hydrogel precursor and compression tests of cylindrical shaped scaffolds. (A) Hydrogel precursors with different bacterial nanocellulose (BNC) contents. (B) Stress-strain curves of cylindrical shaped scaffolds with different BNC contents. (C) Young's modulus of cylindrical-shaped scaffolds with different BNC contents ($n = 7$). ***$P < 0.001$, ****$P < 0.0001$.

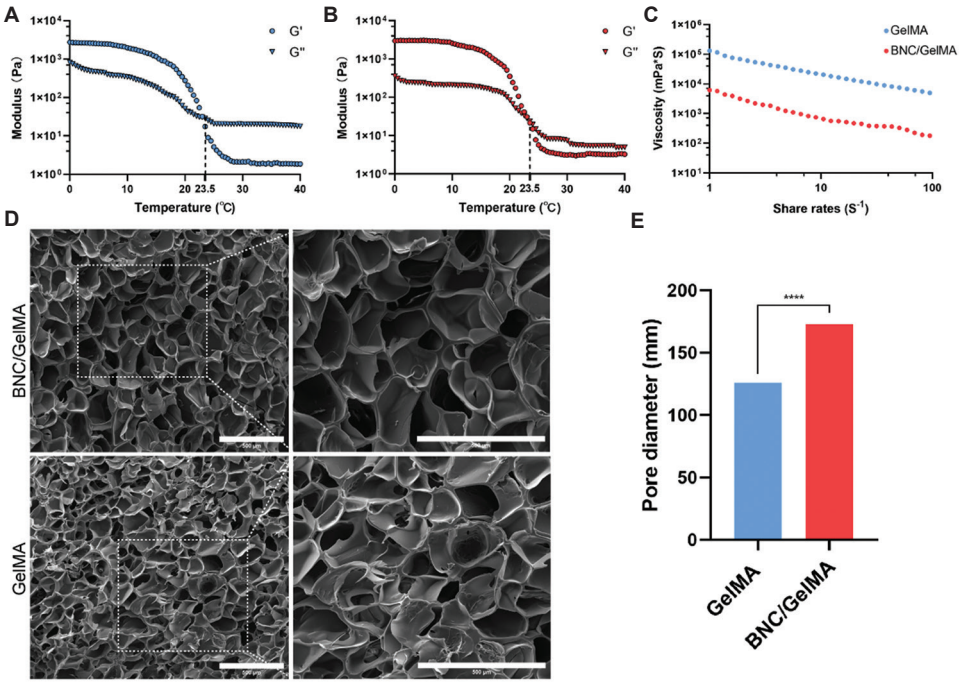

Figure 2. Characterization of hydrogels. (A) Modulus-temperature curve of hydrogel in the gelatin methacryloyl (GelMA) group. (B) Modulus-temperature curve of hydrogel in the bacterial nanocellulose (BNC)/GelMA group. (C) Viscosity-shear rate curve of hydrogels in the GelMA and the BNC/GelMA groups. (D) Scanning electron microscopy examination. (E) Pore size analysis. ****$P < 0.0001$; scale bar: 500 μm.

3.2.2. SEM examination

Both hydrogels in BNC/GelMA group and GelMA group had loose pore structures (Figure 2D). Through further analysis of the pore size, it was found that the average pore size of the hydrogels in BNC/GelMA group and GelMA group was 172.8 ± 54.19 μm and 126.0 ± 35.21 μm, respectively (Figure 2E). The scaffold's pore size of the BNC group was significantly larger than that of the GelMA group ($P < 0.0001$). The loose pore structure may be conducive to the proliferation and migration of cells in the scaffold[38].

3.3. Printability of composite hydrogel

We tested the printability of the hydrogel with nozzles of different inner diameters ranging from 150 μm to 600 μm (Figure 3). The nozzles with inner diameters of 150 μm–210 μm could not be extruded completely, and the nozzles with inner diameters of 250 μm–300 μm were occasionally blocked. When a 400 μm nozzle was used, the hydrogel could be smoothly extruded under pressures above 0.4 bar. Taking the cell viability and printing accuracy into consideration, a 400 μm nozzle and 0.4 – 0.8 bar pressure were used as printing parameters for subsequent experiments.

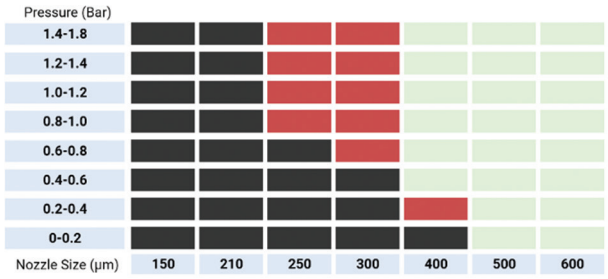

Figure 3. Extrusion test of the bacterial nanocellulose (BNC)/gelatin methacryloyl (GelMA) hydrogel at 21°C with various pressures and nozzles. Black indicates that BNC/GelMA cannot be extruded, red indicates that BNC/GelMA cannot be extruded smoothly, and green indicates that BNC/GelMA can be extruded smoothly.

Different models were used to test the printing formability of the composite hydrogel. The presence of BNC led to the extrusion of a stable filament, which, therefore, contributes to a homogenous diameter distribution alongside the length (Figure 4A). When stacked up to 18 layers, the grid structure formed by the hydrogel could still be seen (Figure 4B). Then, we printed 0.3 times the size of the human jaw model (3.1 × 2.2 × 0.896 cm) (Figure 4C) and 0.4 times the size of the human nose model (2.4 × 1.6 × 0.576 cm) (Figure 4D). The addition of BNC helped obtain uniform lines, complete printing structure, clear surface outline, and high fidelity; these characteristics are essential for the construction of scaffolds with precise morphology.

3.4. Cell viability and migration

3.4.1. Cell viability

The Calcein AM/PI double staining kit was used to stain the live and dead cells on the 1st, 4th, and 7th days after printing to evaluate the cell viability. Most of the cells in the scaffolds were dyed green fluorescence, and only a few cells showed red fluorescence, suggesting high cell viability in the hydrogels (Figure 5A). ImageJ software was used for quantitative analysis of the number of live and dead cells. The percentages of cell viability of the BNC/GelMA group on the 1st, 4th, and 7th days were 96.81 ± 1.541%, 96.12 ± 0.6627%, and 97.34 ± 1.450%, respectively (Figure 5B). There was no significant difference in terms of cell viability between the BNC/GelMA group and the GelMA group ($P > 0.05$).

3.4.2. Cell migration

To explore whether larger internal pores of the BNC/GelMA hydrogel affected the migration of cells in the scaffold, we

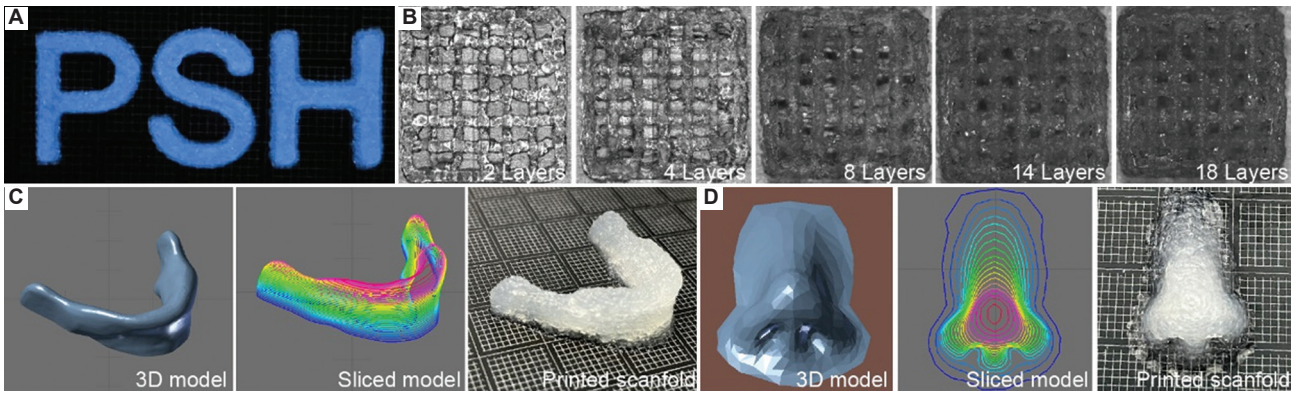

Figure 4. Printability test of bacterial nanocellulose (BNC)/gelatin methacryloyl (GelMA) hydrogel. (A) PSH characters printed with BNC/GelMA hydrogel. (B) Cuboid structure at different layers printed with BNC/GelMA hydrogel. (C) Human mandibular model printed with BNC/GelMA hydrogel. (D) Human nose model printed with BNC/GelMA hydrogel.

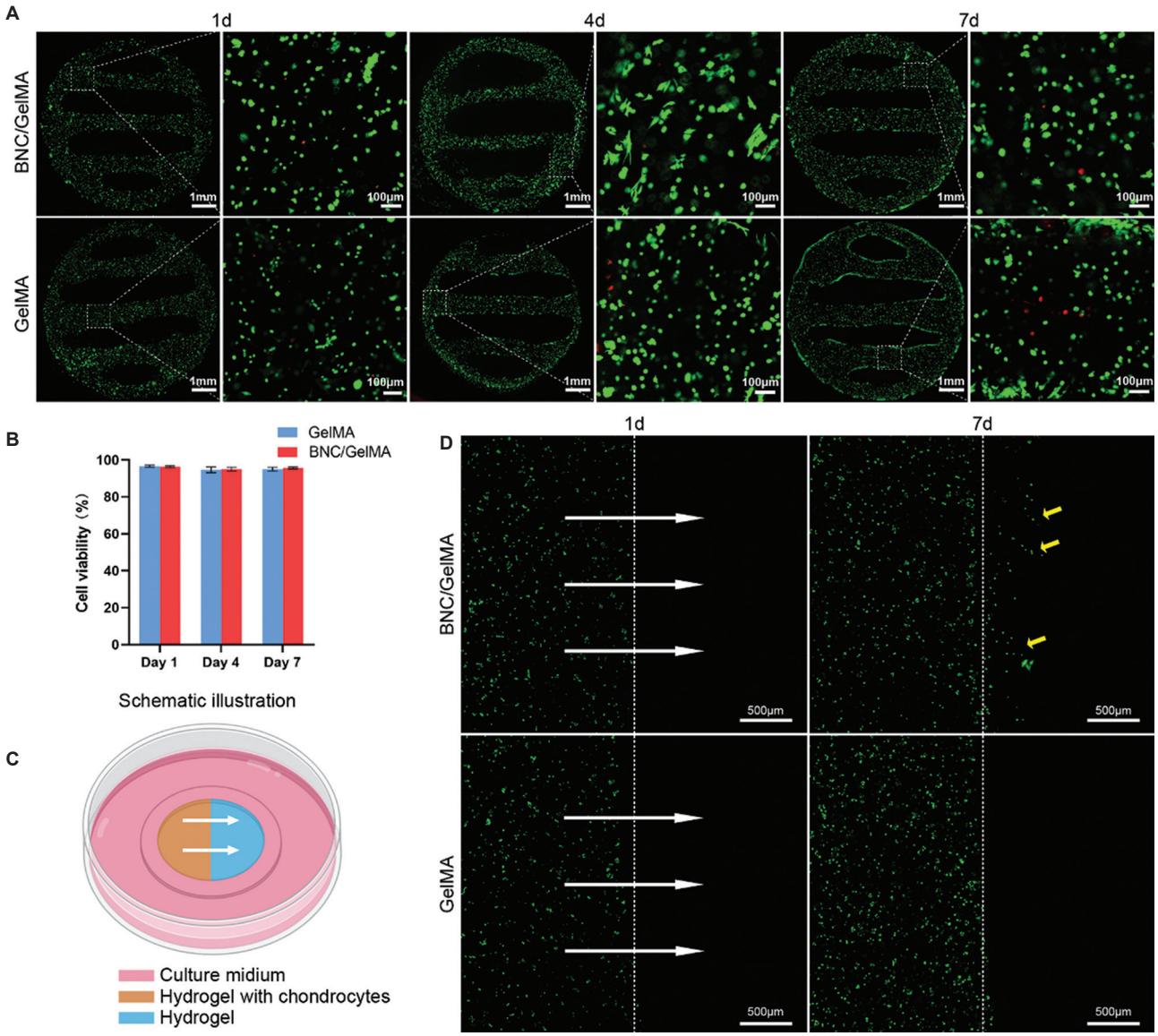

Figure 5. Cell viability and migration tests of hydrogels. (A) The Calcein AM/PI staining of the scaffolds at 1 day, 4 days, and 7 days of *in vitro* culture (green fluorescence representing live cells and red fluorescence representing dead cells). Scale bar: 1 mm. (B) Cell viability of chondrocytes in scaffolds. (C) Schematic illustration of cell migration test. (D) Cell migration evaluated by the Calcein-AM staining under a confocal microscope. The white arrows indicate the direction of cell migration and the yellow arrows indicate migrating cells. Scale bar: 500 μm.

performed cell migration experiments (Figure 5C). Cells in the scaffold of the BNC/GelMA group had obviously migrated to the acellular side on the 7th day, while there was no cell migrating in the GelMA group (Figure 5D). These results suggested that the cells in the BNC/GelMA scaffold had a better migration ability than the cells in the GelMA group. The scaffold of appropriate pore size may justify a higher number of migrating cells in the BNC-containing scaffold[39]. In addition, the previous studies showed that the fiber structure of BNC could promote movement of cells along fiber surfaces[40].

3.5. Cartilage regeneration of the 3D-bioprinted constructs *in vivo*

3.5.1. Mechanical properties of the regenerated cartilage

To explore the cartilage regeneration ability *in vivo* of the composite hydrogel, we implanted the scaffolds into nude mice and took the samples out at the 4th, 8th, 12th, and 24th weeks after implantation. It could be seen from the gross view that white cartilage-like tissue began to form in both BNC/GelMA and GelMA scaffolds from the 8th week after implantation (Figure 6A). At the

24th week, the BNC/GelMA scaffolds were closer to the natural cartilage in gross view. Young's moduli of the constructs in the GelMA group at the 4th, 8th, 12th, and 24th weeks were 84.78 ± 1.239 kpa, 104.0 ± 3.372 kpa, 137.7 ± 2.510 kpa, and 645.2 ± 14.02 kpa, respectively. Meanwhile, Young's moduli of the BNC/GelMA group at the 4th, 8th, 12th, and 24th weeks were 98.24 ± 2.654 kpa, 144.8 ± 0.545 kpa, 187.6 ± 5.907 kpa, and 1332 ± 13.32 kpa, respectively. With the extension of time, Young's modulus of the regenerated cartilage increased gradually in the two groups. From the 4th week, Young's modulus of the BNC/GelMA group was significantly higher than that of the GelMA group ($P < 0.01$). By the 24th week, Young's modulus of the BNC/GelMA group was more than 2 times higher than that of the GelMA group (Figure 6B), which is close to the elastic modulus of the human ear helix (1.41 ± 0.67 MPa)[41].

3.5.2. Quantitative and histological performance

To analyze the extracellular matrix secretion of the regenerated cartilage, we tested the GAG content (Figure 6C) and total collagen content (Figure 6D) of the samples. At the 4th, 8th, 12th, and 24th week, the GAG contents in BNC/GelMA group were 5.349 ± 0.2706 mg/g, 6.928 ± 0.3651 mg/g, 11.90 ± 0.4840 mg/g, and 31.99 ± 0.6753 mg/g, respectively, whereas the GAG contents in GelMA group were 5.268 ± 0.2009 mg/g, 6.564 ± 0.3038 mg/g, 10.04 ± 0.8624 mg/g, and 24.10 ± 0.7412 mg/g, respectively. The GAG content of the regenerated cartilage in the two groups gradually increased from the 4th week. By the 12th and 24th weeks, the GAG content in the regenerated cartilage of the BNC/GelMA group was significantly higher than that of the GelMA group ($P < 0.001$), which was closer to the natural rabbit ear cartilage (44.31 ± 0.4858 mg/g). We measured the content of hydroxyproline to estimate the total collagen content. The results showed that the total collagen content also gradually increased over time and attained the expression level of natural rabbit ear cartilage collagen at the 24th week after implantation. However, there was no significant difference between the two groups at all the tested time points ($P > 0.05$).

The mechanical results were in line with the GAG content results. A previous study has shown that the compressive capacity in cartilage tissue is mainly attributed to the GAG[42], which was consistent with our results.

We further performed H&E, Alcian blue, and Safranine-O staining for histological evaluation. It could be seen from the H&E staining that from the 4th week, cartilage lacunae had formed in both BNC/GelMA and GelMA scaffolds, and with the extension of time, the staining of cartilage extracellular matrix in the scaffolds became deeper in color, as shown in Alcian blue and Safranine-O staining results (Figure 7). It could be seen in the gross specimens and histological staining results that the hydrogels were still present in the samples at 24 weeks. A previous study on the degradation of GelMA showed that GelMA could remain in collagenase solution for 10 days[43], but no relevant reports on the degradation of GelMA and BNC *in vivo* were found. However, the hydrogel degrades more slowly in nude mice due to

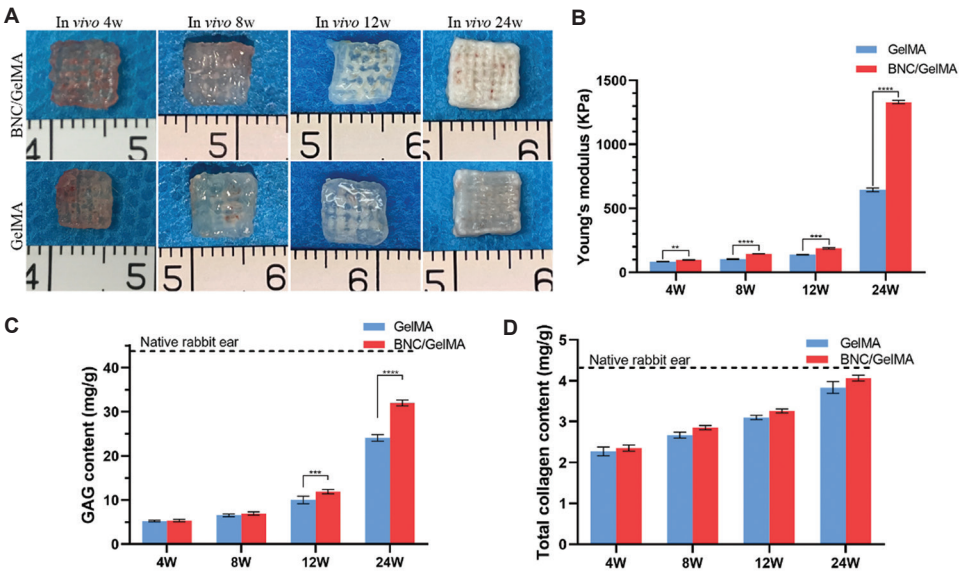

Figure 6. Gross observation and biomechanical and biochemical tests of regenerated cartilage *in vivo*. (A) Gross view of regenerated cartilage at weeks 4, 8, 12, and 24 after implantation. (B) Young's modulus of regenerated cartilage ($n = 3$). (C) Glycosaminoglycan content of regenerated cartilage ($n = 3$). (D) Total collagen content of regenerated cartilage ($n = 3$). $^{**}P < 0.01$, $^{***}P < 0.001$, $^{****}P < 0.0001$.

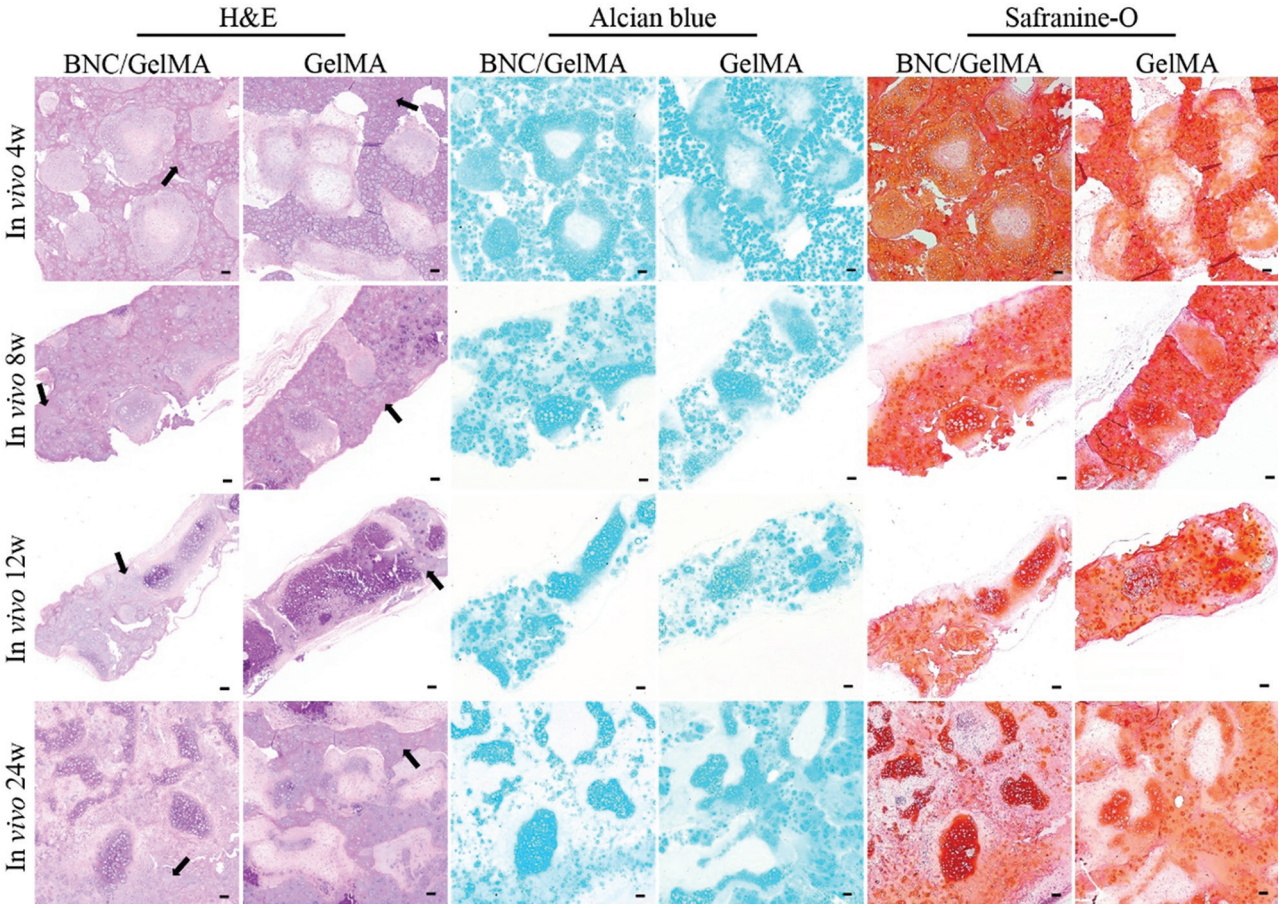

Figure 7. Histological examination of regenerated cartilage. H&E, Alcian blue, and Safranine-O staining of regenerated cartilage at 4th, 8th, 12th, and 24th weeks of *in vivo* culture. The black arrows indicate undegraded hydrogels. Scale bar: 100 μm.

the lack of immunity. Therefore, experiments using hydrogels with fluorescent labeling and large animals with immunity are needed to evaluate the degradation of hydrogels *in vivo*.

3.5.3. 3D bioprinting and regeneration of ear-shaped cartilage constructs

To detect the feasibility of morphological maintenance of the composite hydrogel, we constructed a scaffold with 0.4 times the size of a normal human ear by 3D bioprinting using the composite hydrogel and rabbit auricular chondrocytes (Video clip 1). The cartilage scaffolds were superimposed layer by layer under the 3D printer, and finally, 22 layers were printed (Figure 8A). The printed human ear-shaped scaffold was basically consistent with the 3D model, and there was no material collapse during the printing process (Figure 8B). The live/dead staining results demonstrated that the cells embedded in hydrogels had good viability (Figure 8C). Subsequently, we implanted the scaffold subcutaneously in nude mice (Figure 8D) and collected it at 24 weeks after implantation. The regenerated cartilage, which was well maintained and in condition similar to before implantation (Figure 8E), showed a milky white cartilage appearance (Figure 8F) and had good elasticity (Supplement 2). Histological examination revealed the formation of a considerable amount of cartilage-specific extracellular matrix indicated by Safranine-O and Alcian blue staining and the formation of typical lacunae structure indicated by H&E staining (Figure 8G).

In this study, BNC/GelMA composite hydrogel was used to regenerate ear cartilage. We confirmed that a small amount of BNC could greatly improve the mechanical strength of GelMA hydrogel materials. In addition, the cell viability in the hydrogels was still above 95% on day 7, which was higher than in a previous study, in which Markstedt *et al.* constructed ear cartilage scaffolds with alginate/nano-cellulose hydrogel through 3D bioprinting, and the cell viability on the 7th day was only 85.7%[44]. In another study, Martínez *et al.* proposed the use of a nanocellulose hydrogel for 3D bioprinting

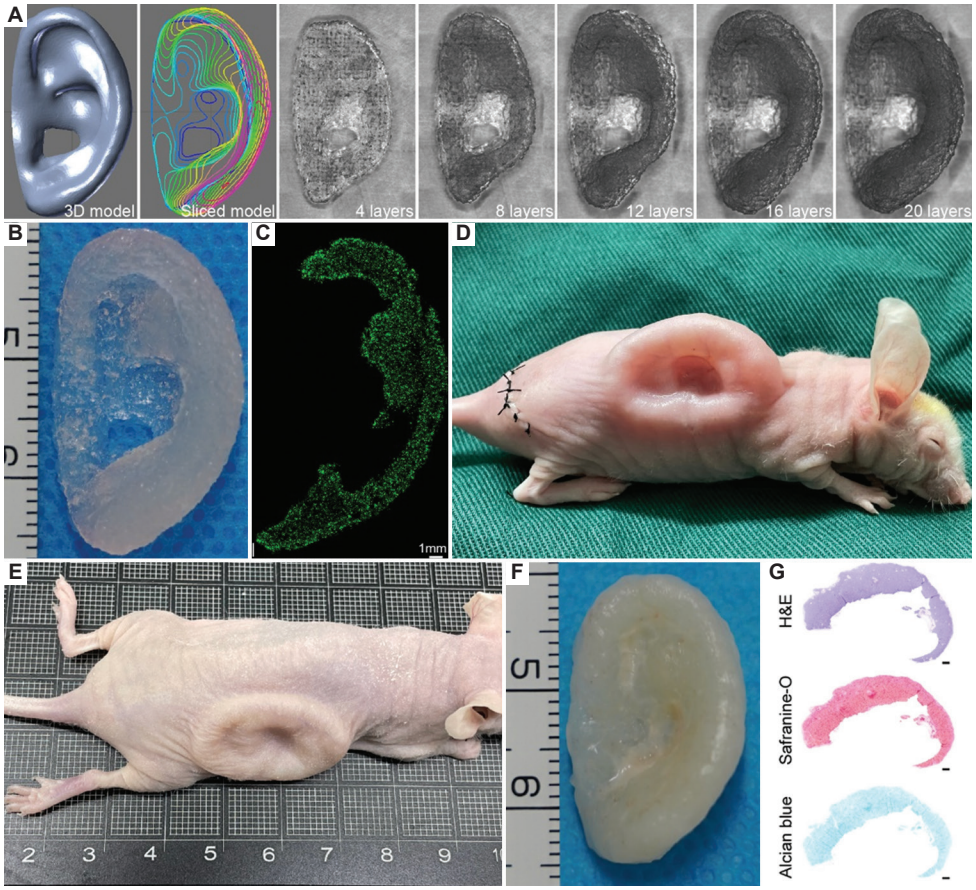

Figure 8. 3D bioprinting of ear-shaped cartilage using bacterial nanocellulose (BNC)/gelatin methacryloyl (GelMA) bio-ink. (A) 3D-bioprinted ear-shaped scaffold with BNC/GelMA bio-ink. (B) Ear-shaped scaffold laden with chondrocytes before implantation. (C) Calcein AM/PI staining of the ear-shaped scaffold. (D) Ear-shaped scaffold immediately after implantation in nude mice. (e) Ear-shaped scaffold after implantation in nude mice after 24 weeks of culture *in vivo*. (F) Morphology of the ear-shaped scaffold after 24 weeks of culture *in vivo.* (G) H&E staining, Safranine-O, and Alcian blue staining of the scaffold after 24 weeks of culture *in vivo*. Scale bar: 1 mm.

to regenerate auricular cartilage, and the cell viability after 3D bioprinting was only 70.9 ± 7.2%[45]. In addition, it should be noted that the BNC-containing hydrogel promoted cell migration, which is an important cellular feature for tissue morphogenesis. The most important criterion for testing whether a biomaterial is suitable for tissue engineering is to evaluate tissue regeneration *in vivo*[11]. We implanted the chondrocyte-laden 3D-bioprinted scaffolds into nude mice and cultured them for 24 weeks *in vivo*. The results demonstrated that the composite hydrogel was beneficial to the GAG secretion in regenerated cartilage, and its biomechanical properties were significantly enhanced, which was close to the Young's modulus of human ear cartilage. Moreover, a precise ear-shaped construct was bioprinted, and the cartilage with 3D morphology was regenerated successfully *in vivo*, which further verified the feasibility of applying BNC-reinforced GelMA hydrogels in auricular cartilage tissue engineering. Certainly, future studies in large animal models are required to verify its potential in preclinical applications.

4. Conclusions

A BNC/GelMA composite hydrogel was prepared in this study. Compared with 10% GelMA, the 0.375% BNC composite hydrogel has superior mechanical properties as well as better printability and cell migration ability. Auricular cartilage was regenerated in nude mice using chondrocyte-laden BNC/GelMA hydrogel. The cartilage tissue regenerated by the hydrogel had higher GAG content and better biomechanical properties. Finally, the ear-shaped construct was bioprinted with composite hydrogels, and the cartilage tissue was successfully regenerated *in vivo*. Although the superiority of the composite hydrogel needs to be further verified in large animal experiments, this study offers insights into using an alternative material coupled with detailed technical parameters in the construction of precise-shaped cartilage.

Acknowledgments

None.

Funding

This work was financially supported by the Chinese Academy of Medical Sciences Innovation Fund for Medical Sciences (2021-I2M-1-052, 2017-I2M-1-007) and the National Natural Science Foundation of China (81871575).

Conflict of interest

The authors declare no competing financial interest.

Author contributions

Conceptualization: Jinshi Zeng, Xia Liu, Qinghua Yang, and Haiyue Jiang
Data curation: Jinshi Zeng, Litao Jia, and Zhuoqi Chen
Funding acquisition: Xia Liu and Haiyue Jiang
Investigation: Jinshi Zeng, Xia Liu, and Qinghua Yang
Methodology: Jinshi Zeng, Litao Jia, and Xia Liu
Visualization: Jinshi Zeng, Di Wang, and Wenshuai Liu
Supervision: Qinghua Yang and Haiyue Jiang
Writing – original draft: Jinshi Zeng
Writing – review & editing: Xia Liu.

Ethics approval and consent to participate

Not applicable.

Consent for publication

Not applicable.

Availability of data

The data that used during this study are available from the corresponding author upon reasonable request.

References

1. Tanzer RC, 1961, Total reconstruction of the external auricle. *Arch Otolaryngol*, 73: 64–68.

   https://doi.org/10.1001/archotol.1961.00740020068008

2. Brent B, 1974, Ear reconstruction with an expansile framework of autogenous rib cartilage. *Plast Reconstr Surg*, 53: 619–628.

   https://doi.org/10.1097/00006534-197406000-00001

3. Conway H, Neumann CG, Gelb J, *et al*., 1948, Reconstruction of the external ear. *Ann Surg*, 128: 226–239.

   https://doi.org/10.1097/00000658-194808000-00005

4. Brent B, Tanzer RC, Rueckert F, *et al*., 1992, Auricular repair with autogenous rib cartilage grafts. *Plast Reconstr Surg*, 90: 375–376.

   https://doi.org/10.1097/00006534-199209000-00002

5. Nagata S, 1993, A new method of total reconstruction of the auricle for microtia. *Plast Reconstr Surg*, 92: 187–201.

   https://doi.org/10.1097/00006534-199308000-00001

6. Brent B, 1999, Technical advances in ear reconstruction with autogenous rib cartilage grafts: Personal experience with 1200 cases. *Plast Reconstr Surg*, 104: 319–334.

   https://doi.org/10.1097/00006534-199908000-00001

7. Zhang Q, Zhang R, Xu F, *et al*., 2009, Auricular reconstruction for microtia: personal 6-year experience based on 350 microtia ear reconstructions in china. *Plast Reconstr Surg*, 123: 849–858.

   https://doi.org/10.1097/PRS.0b013e318199f057

8. Cao Y, Vacanti JP, Paige KT, *et al*., 1997, Transplantation of chondrocytes utilizing a polymer-cell construct to produce tissue-engineered cartilage in the shape of a human ear. *Plast Reconstr Surg*, 100: 297–302.

   https://doi.org/10.1097/00006534-199708000-00001

9. Zhou G, Jiang H, Yin Z, *et al*., 2018, *In vitro* regeneration of patient-specific ear-shaped cartilage and its first clinical application for auricular reconstruction. *EBioMedicine*, 28:287–302.

   https://doi.org/10.1016/j.ebiom.2018.01.011

10. Sterodimas A, de Faria J, Correa WE, *et al*., 2009, Tissue engineering and auricular reconstruction: A Review. *J Plast Reconstr Aesthet Surg*, 62: 447–452.

    https://doi.org/10.1016/j.bjps.2008.11.046

11. Jia L, Zhang Y, Yao L, *et al*., 2020, Regeneration of human-ear-shaped cartilage with acellular cartilage matrix-based biomimetic scaffolds. *Appl Mater Today*, 20: 100639.

    https://doi.org/10.1016/j.apmt.2020.100639

12. Ning L, Mehta R, Cao C, *et al*., 2020, Embedded 3D bioprinting of gelatin methacryloyl-based constructs with highly tunable structural fidelity. *ACS Appl Mater Interfaces*, 12: 44563–44577.

    https://doi.org/10.1021/acsami.0c15078

13. Duin S, Schutz K, Ahlfeld T, *et al*., 2019, 3D Bioprinting of functional islets of langerhans in an alginate/methylcellulose hydrogel blend. *Adv Healthc Mater*, 8: e1801631.

    https://doi.org/10.1002/adhm.201801631

14. Rakin RH, Kumar H, Rajeev A, *et al*., 2021, Tunable metacrylated hyaluronic acid-based hybrid bioinks for stereolithography 3D bioprinting. *Biofabrication*, 13: 044109.

    https://doi.org/10.1088/1758-5090/ac25cb

15. Rastogi P, Kandasubramanian B, 2019, Review of alginate-based hydrogel bioprinting for application in tissue engineering. *Biofabrication*, 11: 042001.

    https://doi.org/10.1088/1758-5090/ab331e

16. Levett PA, Melchels FP, Schrobback K, *et al.*, 2014, A biomimetic extracellular matrix for cartilage tissue engineering centered on photocurable gelatin, hyaluronic acid and chondroitin sulfate. *Acta Biomater*, 10: 214–223.

https://doi.org/10.1016/j.actbio.2013.10.005

17. Gungor-Ozkerim PS, Inci I, Zhang YS, *et al.*, 2018, Bioinks for 3D bioprinting: An overview. *Biomater Sci*, 6: 915–946.

https://doi.org/10.1039/c7bm00765e

18. Huang J, Xiong J, Wang D, *et al.*, 2021, 3D bioprinting of hydrogels for cartilage tissue engineering. *Gels*, 7: 144.

https://doi.org/10.3390/gels7030144

19. Kang HW, Lee SJ, Ko IK, *et al.*, 2016, A 3D bioprinting system to produce human-scale tissue constructs with structural integrity. *Nat Biotechnol*, 34: 312–319.

https://doi.org/10.1038/nbt.3413

20. Sun Y, You Y, Jiang W, *et al.*, 2019, 3D-bioprinting a genetically inspired cartilage scaffold with GDF5-conjugated bmsc-laden hydrogel and polymer for cartilage repair. *Theranostics*, 9: 6949–6961.

https://doi.org/10.7150/thno.38061

21. Matai I, Kaur G, Seyedsalehi A, *et al.*, 2020, Progress in 3D bioprinting technology for tissue/organ regenerative engineering. *Biomaterials*, 226: 119536.

https://doi.org/10.1016/j.biomaterials.2019.119536

22. Klotz BJ, Gawlitta D, Rosenberg A, *et al.*, 2016, Gelatin-methacryloyl hydrogels: Towards biofabrication-based tissue repair. *Trends Biotechnol*, 34: 394–407.

https://doi.org/10.1016/j.tibtech.2016.01.002

23. Yang R, Chen F, Guo J, *et al.*, 2020, Recent advances in polymeric biomaterials-based gene delivery for cartilage repair. *Bioact Mater*, 5: 990–1003.

https://doi.org/doi.org/10.1016/j.bioactmat.2020.06.004

24. Yue K, Trujillo-de Santiago G, Alvarez MM, *et al.*, 2015, Synthesis, properties, and biomedical applications of gelatin methacryloyl (gelma) hydrogels. *Biomaterials*, 73: 254–271.

https://doi.org/10.1016/j.biomaterials.2015.08.045

25. Bhamare N, Tardalkar K, Parulekar P, *et al.*, 2021, 3D printing of human ear pinna using cartilage specific ink. *Biomed Mater*, 16: 055008.

https://doi.org/10.1088/1748-605X/ac15b0

26. Taghipour YD, Hokmabad VR, Del Bakhshayesh AR, *et al.*, 2020, The application of hydrogels based on natural polymers for tissue engineering. *Curr Med Chem*, 27: 2658–2680.

https://doi.org/10.2174/0929867326666190711103956

27. Pertile RA, Moreira S, Gil da Costa RM, *et al.*, 2012, Bacterial cellulose: Long-term biocompatibility studies. *J Biomater Sci Polym Ed*, 23: 1339–1354.

https://doi.org/10.1163/092050611X581516

28. McKenna BA, Mikkelsen D, Wehr JB, *et al.*, 2009, Mechanical and structural properties of native and alkali-treated bacterial cellulose produced by *gluconacetobacter xylinus* strain ATCC 53524. *Cellulose*, 16: 1047–1055.

https://doi.org/10.1007/s10570-009-9340-y

29. Athukoralalage SS, Balu R, Dutta NK, *et al.*, 2019, 3D bioprinted nanocellulose-based hydrogels for tissue engineering applications: A brief review. *Polymers* (*Basel*), 11: 898.

https://doi.org/10.3390/polym11050898

30. Singhsa P, Narain R, Manuspiya H, 2017, Bacterial cellulose nanocrystals (BCNC) preparation and characterization from three bacterial cellulose sources and development of functionalized bcncs as nucleic acid delivery systems. *ACS Appl Nano Mater*, 1:209–221.

https://doi.org/10.1021/acsanm.7b00105

31. Duchi S, Onofrillo C, O'Connell CD, *et al.*, 2017, Handheld co-axial bioprinting: application to *in situ* surgical cartilage repair. *Sci Rep*, 7: 5837.

https://doi.org/10.1038/s41598-017-05699-x

32. Jia L, Hua Y, Zeng J, *et al.*, 2022, Bioprinting and regeneration of auricular cartilage using a bioactive bioink based on microporous photocrosslinkable acellular cartilage matrix. *Bioact Mater*, 16: 66–81.

https://doi.org/10.1016/j.bioactmat.2022.02.032

33. Xu Y, Zhou J, Liu C, *et al.*, 2021, Understanding the role of tissue-specific decellularized spinal cord matrix hydrogel for neural stem/progenitor cell microenvironment reconstruction and spinal cord injury. *Biomaterials*, 268: 120596.

https://doi.org/10.1016/j.biomaterials.2020.120596

34. Hua Y, Xia H, Jia L, *et al.*, 2021, Ultrafast, tough, and adhesive hydrogel based on hybrid photocrosslinking for articular cartilage repair in water-filled arthroscopy. *Sci Adv*, 7: eabg0628.

https://doi.org/10.1126/sciadv.abg0628

35. Mendoza L, Batchelor W, Tabor RF, *et al.*, 2018, Gelation mechanism of cellulose nanofibre gels: A colloids and interfacial perspective. *J Colloid Interface Sci*, 509: 39–46.

https://doi.org/10.1016/j.jcis.2017.08.101

36. Fourati Y, Tarres Q, Delgado-Aguilar M, *et al.*, 2021, Cellulose nanofibrils reinforced PBAT/TPS blends: Mechanical and rheological properties. *Int J Biol Macromol*, 183: 267–275.

https://doi.org/10.1016/j.ijbiomac.2021.04.102

37. Fan Y, Yue Z, Lucarelli E, *et al.*, 2020, Hybrid printing using cellulose nanocrystals reinforced GelMA/HAMA hydrogels for improved structural integration. *Adv Healthc Mater*, 9: e2001410.

https://doi.org/10.1002/adhm.202001410

38. Rathan S, Dejob L, Schipani R, *et al*., 2019, Fiber reinforced cartilage ECM functionalized bioinks for functional cartilage tissue engineering. *Adv Healthc Mater*, 8: e1801501.

https://doi.org/10.1002/adhm.201801501

39. Loh E, Fauzi MB, Ng MH, *et al*., 2018, Cellular and molecular interaction of human dermal fibroblasts with bacterial nanocellulose composite hydrogel for tissue regeneration. *ACS Appl Mater Interfaces*, 10: 39532–39543.

https://doi.org/10.1021/acsami.8b16645

40. Zhang P, Chen L, Zhang Q, *et al*., 2016, Using *in situ* nanocellulose-coating technology based on dynamic bacterial cultures for upgrading conventional biomedical materials and reinforcing nanocellulose hydrogels. *Biotechnol Prog*, 32:1077–1084.

https://doi.org/10.1002/btpr.2280

41. Griffin MF, Premakumar Y, Seifalian AM, *et al*., 2016, Biomechanical characterisation of the human auricular cartilages; implications for tissue engineering. *Ann Biomed Eng*, 44:3460–3467.

https://doi.org/10.1007/s10439-016-1688-1

42. Qasim M, Chae DS, Lee NY, 2019, Advancements and frontiers in nano-based 3D and 4D scaffolds for bone and cartilage tissue engineering. *Int J Nanomed*, 14:4333–4351.

https://doi.org/10.2147/IJN.S209431

43. Zhao X, Lang Q, Yildirimer L, *et al*., 2016, Photocrosslinkable gelatin hydrogel for epidermal tissue engineering. *Adv Healthc Mater*, 5:108–118.

https://doi.org/10.1002/adhm.201500005

44. Markstedt K, Mantas A, Tournier I, *et al*., 2015, 3D bioprinting human chondrocytes with nanocellulose-alginate bioink for cartilage tissue engineering applications. *Biomacromolecules*, 16: 1489–1496.

https://doi.org/10.1021/acs.biomac.5b00188

45. Ávila HM, Schwarz S, Rotter N, *et al*., 2016, 3D bioprinting of human chondrocyte-laden nanocellulose hydrogels for patient-specific auricular cartilage regeneration. *Bioprinting*, 1–2: 22–35.

https://doi.org/10.1016/j.bprint.2016.08.003